Received: March 14, 2024. Revised: May 29, 2024.

INASS

International Journal of
Intelligent Engineering & Systems

http://www.inass.org/

Enhanced Brain Tumor MRI Scan Reconstruction via the EI-Fusion-Net Model

BSH. Shayeez Ahamed[1,2] Radhika Baskar[3]* G Nalinipriya[4]

[1]*Department of Computer Science and Engineering, Saveetha School of Engineering, Saveetha Institute of Medical and Technical Sciences, Saveetha University, Chennai, India*
[2]*Madanapalle Institute of Technology & Science, Madanapalli, Andhra Pradesh, India*
[3]*Department of Electronics and Communication Engineering, Saveetha School of Engineering, Saveetha Institute of Medical and Technical Sciences, Saveetha University, Chennai, India*
[4]*Department of IT, Saveetha Engineering College, Chennai, Tamilnadu, India*
* Corresponding author's Email: radhikabaskar@saveetha.com

Abstract: Our novel methodology for tumor identification improves accuracy and efficiency significantly by utilizing advanced techniques. Using the BRATS dataset, we combine Maximum A Posteriori (MAP) optimization for pixel extraction, Wiener deconvolution, and the EI-Fusion-Net deep neural network. Additionally, preprocessing techniques such as resizing, grayscale conversion, and Gaussian filtering are used to improve image quality. For better results, our novel image fusion EI-Fusion-Net approach uses specific wavelet transform techniques and a fusion network architecture capable of capturing both spatial and temporal information. Indeed, our findings show remarkable performance metrics, with a peak signal-to-noise ratio (PSNR) of 48.42 dB and a structural similarity index (SSIM) of 0.992, which outperform those of existing methods on the BRATS dataset. This demonstrates the EI-Fusion-Net model's ability to effectively combine diverse data sources, resulting in promising advances in brain tumor detection via refined medical image processing techniques.

Keywords: BRATS, Brain scan images, MRI, Wiener de convolution, Convolutional neural network.

1. Introduction

Medical imaging is essential in modern healthcare, helping to diagnose and treat a variety of medical conditions [1-3]. Among these imaging modalities, Magnetic Resonance Imaging (MRI) stands out as an operative tool for visualizing internal structures in high detail and contrast [4, 5]. MRI scans of the brain, in particular, are widely used to diagnose neurological disorders such as brain tumours [6]. However, noise, artifacts, and blurring can all have an impact on the quality of MRI images, making accurate diagnosis and treatment planning more difficult [7-9]. Image reconstruction techniques seek to progress the eminence of MRI images by increasing resolution, decreasing noise, and removing artifacts [10]. These techniques are essential for extracting meaningful information from medical images [12]. In the context of brain tumor MRI scans [13, 14], reconstruction techniques are critical for visualizing tumor morphology [15], defining tumor boundaries, and monitoring treatment response [16].

Our research methodology includes a series of critical steps, that are designed to optimize the reconstruction process and improve the fidelity of MRI images. The proposed methodology begins with retrieving brain tumor MRI images from the BRATS dataset, which is a popular repository of brain tumor images for research purposes. These images are then preprocessed, including resizing and grayscale conversion [17], to allow for further analysis. Importantly, our deep learning model is trained on an augmented dataset derived from the BRATS dataset, resulting in consistent performance across a wide range of images. Our methodology continues with Gaussian filtering [18] to reduce noise and Wiener deconvolution to effectively reverse blurring effects,

resulting in a reconstructed image with increased clarity and detail.

Notably, our proposed methodology has several advantages over current methods. To begin, by combining deep learning and advanced image processing algorithms, we achieve superior image quality and computational efficiency. Furthermore, our methodology is robust and adaptable, allowing us to deal with a wide range of imaging conditions and tumor morphology variations. Furthermore, we introduce new features to our methodology, such as additional Gaussian filtering and blind deconvolution, to improve image quality and reduce artifacts. The use of the Daubechies wavelet transform for image fusion, as well as the Long Short-Term Memory Convolutional Neural Network (LSTM-CNN) architecture, are innovative contributions to the field of medical image processing.

In supposition, our findings highlight the critical need for improved image reconstruction techniques in the context of brain tumor MRI scans. The proposed methodology has great potential for advancing the field of medical imaging and facilitating more accurate diagnoses and treatment planning for patients with brain tumours.

The paper is organised as follows: Section 1 introduces Brain MRI Imaging and summarises our contributions. Section 2 examines related works in MRI image reconstruction. Section 3 discusses our methodology, which includes data preprocessing, denoising, deconvolution, and image fusion. Section 4 contains results and analysis, including quality metrics and computational assessments. Section 5 concludes the paper by summarising our contributions and discussing potential future directions in medical imaging.

2. Literature review

Xu et al. [19] developed the SepGAN framework, which utilizes depthwise separable convolution as a key element to improve the accuracy of MRI reconstruction. The new method produced impressive outcomes, with a PSNR of 44.22 dB and a SSIM of 0.985. Nevertheless, SepGAN has specific constraints despite its favorable results. The computational complexity of this may restrict its use in real-time situations or resource-limited settings. Furthermore, the effectiveness of SepGAN may differ based on the unique attributes of the input MRI data, requiring additional validation across various datasets and thorough comparison with established techniques to comprehensively evaluate its reliability and applicability.

Sabina et al. [20] developed the Deep Residual Feature Distillation Channel Attention Network (DRFDCAN) to improve high-frequency features important for detailed medical diagnostics without compromising image quality. The network attains a PSNR of 34.20 dB and a SSIM of 0.9468. Despite its promising performance, DRFDCAN may have limitations in scalability to larger datasets and generalization to diverse imaging modalities, potentially hindering its applicability in real-world medical imaging scenarios.

Li et al. [21] proposed the Global Attention-enabled Texture Enhancement Network (GATE-Net) to address the problem of reconstructing highly undersampled MR images, with a PSNR of 36.81 dB and an SSIM of 0.978. By incorporating global attention mechanisms, GATE-Net focuses on improving textural details that are critical for accurate image reconstruction. It may face difficulties in generalizing to a variety of MR imaging scenarios and acquisition protocols.

Zhou and colleagues [22] projected a novel approach called Multimodal Feature Fusion with deep neural networks, which combines three critical components. This network architecture aims to effectively combine features from various modalities while facilitating latent feature learning. Notably, the method yields a Structural Similarity Index (SSIM) of 0.89 and a Peak Signal-to-Noise Ratio (PSNR) of 29.46. Potential overfitting issues and the need for significant computational resources for training and inference are basic limitations that may come.

Ahmad et al. [23] presented a novel Generative Adversarial Network (GAN) architecture designed for medical image generation where this method uses a reconstruction convolutional layer. Impressively, the method achieves a PSNR of 38.83 dB and a SSIM of 0.95. It may face limitations such as mode collapse and the possibility of artifacts in generated images, which could limit its utility in medical diagnostics and decision-making processes.

Hossain et al. [24] proposed a new method for MRI reconstruction called the Fully Dense Attention CNN (FDA-CNN), which incorporates fully dense connectivity and attention mechanisms into the standard U-Net model. This enhancement resulted in significant improvements, with maximum PSNR values of 41.75 dB and a SSIM of 0.98. However, a major limitation of the U-Net method, including its FDA-CNN variant, is its susceptibility to overfitting, which may limit its generalizability.

Shilpa et al. [25] developed a new hybrid compressive sensing algorithm for reconstruction. This method aims to efficiently reconstruct signals from heavily undersampled data. The reconstruction

yielded impressive results, with a PSNR of 41.68 dB and a SSIM of 0.975. However, one significant limitation of this method is its computational complexity, particularly in training the neural network component and the iterative process of L1 minimization.

Zhou Z et al. [26] proposed the MRI-based Brain Tumor Super-Resolution Generative Adversarial Network (MRBT-SR-GAN. This network uses GANs to achieve super-resolution, which improves fine detail in the images. Notably, the reconstruction process produces an average PSNR of 29.42 and a SSIM of 0.986, demonstrating its ability to preserve image quality. Its performance may be limited when applied to images containing various tumor types, sizes, or imaging artifacts.

The challenge in medical image processing, particularly brain tumor detection and reconstruction with MRI scans, is to achieve high accuracy and efficiency while maintaining image quality. Despite promising techniques such as SepGAN, DRFDCAN, and GATE-Net, limitations in scalability, generalization, and computational complexity remain. The goal is to develop novel methodologies that integrate diverse data sources, optimize learning parameters, and improve image resolution while addressing overfitting issues and ensuring applicability across various datasets and imaging modalities. Advancements such as the EI-Fusion-Net model highlight the need for innovative solutions that outperform current accuracy and efficiency benchmarks in image reconstruction.

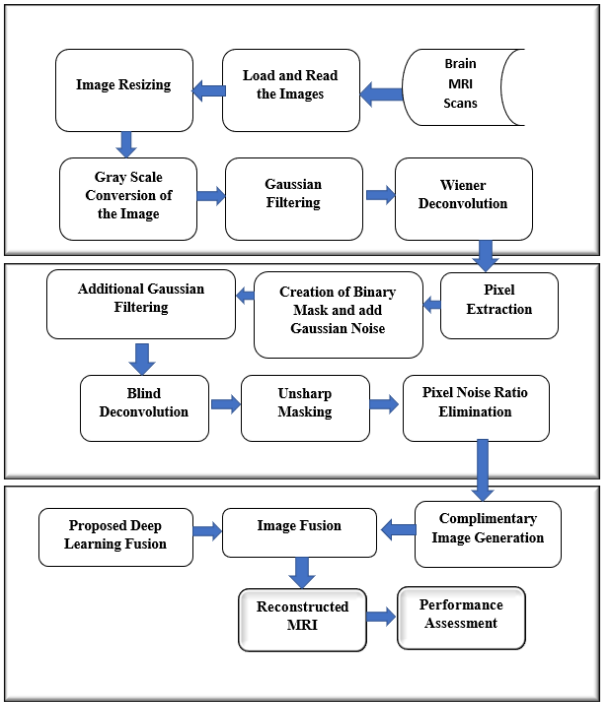

Figure. 1 Proposed block diagram for image reconstruction

3. Methodology

The research methodology, as illustrated in Fig. 1, encompasses a series of essential steps aimed at enhancing the quality of brain tumor MRI scan images for reconstruction purposes. It commences by retrieving images from the BRATS dataset [27], followed by resizing and converting them into grayscale. The proposed fusion based deep learning model was trained on an augmented dataset of 3000 samples derived from the BRATS dataset's initial 300 images. Subsequent Gaussian filtering reduces noise, while Wiener deconvolution effectively reverses blurring effects. The reconstructed image is subsequently displayed and rigorously evaluated, encompassing parameters such as computational time and quality metrics. This comprehensive methodology significantly contributes to the field of medical mage processing, particularly in the context of reconstructing brain tumor MRI scan images.

Retrieve an image (f(x, y)) from an augmented dataset of BRATS [27] via Kaggle. Resize the loaded image (f(x, y)) to a desired size, resulting in a new image g(x, y). The resizing operation can be represented mathematically as follows:

$$g(x,y) = Resize(f(x,y), Width, Height) \quad (1)$$

Where g(x, y) is the resized image, f(x, y) is the original image, Width and Height represent the desired dimensions for resizing.

Apply a color mapping function to convert the resized image into grayscale. The function can be represented as:

$$gray(x,y) = ColorMapping(g(x,y)) \quad (2)$$

Where gray (x, y) is the resulting grayscale image

Perform Gaussian filtering on the grayscale image to smooth and reduce noise. The Gaussian filtering operation can be represented mathematically as a convolution of the grayscale image (gray (x, y)) with a Gaussian kernel ($G_F(x,y)$)).

$$S_m(x,y) = gray(x,y) \circledast G_F(x,y) \quad (3)$$

Where $S_m(x,y)$ is the resulting smoothed image., gray(x, y) is the grayscale image obtained in the previous step, $G_F(x,y)$ is the Gaussian kernel,

The Gaussian kernel is defined by the following equation:

$$G_{F(x,y)} = \left(\frac{1}{(2\ \pi\ \sigma^2)}\right) e^{-\left(\frac{(x^2+y^2)}{(2\ \sigma^2)}\right)} \quad (4)$$

Where (x, y) are the coordinates in the kernel, σ (sigma) controls the spread or standard deviation of the Gaussian distribution, π (pi) is the mathematical constant, e is the base of the natural logarithm.

Apply Wiener deconvolution to the filtered image. Mathematically, Wiener deconvolution can be represented as follows:

$$G(u,v) = \frac{\overline{H}(u,v) \cdot F(u,v)}{|H(u,v)|^2 + K.N(u,v)} \quad (5)$$

Where G(u,v) is the estimated Fourier transform of the original image. $\overline{H}(u,v)$ is the complex conjugate of the PSF's frequency response. K is a constant (Wiener regularization parameter), $|H(u,v)|^2$ represents the magnitude of the PSF's frequency response squared. N(u,v) represents the noise power spectral density.

$$g_r(x,y) = F^{-1}[G(u,v)] \quad (6)$$

Where g_r (x,y) is the restored image in spatial domain, which is visually interpretable.

Mathematically, MAP pixel extraction can be represented as follows:

$$E(gr) = -log(P(gr \mid observed\ data)) - log(P(gr \mid prior)) \quad (7)$$

Where, *E*(*gr*) is the energy or cost associated with the restored image *gr*(*x*,*y*), *P*(*gr* | observed data) represents the likelihood term, which measures how well the restored image fits the observed data, *P*(*gr*| prior) represents the prior term, which encodes prior knowledge or constraints on the image.

The MAP method aims to find the values of *gr* (*x*,*y*) that minimize the objective function (*E*(*gr*):)

$$\overline{g_r} = \arg\min E(gr) \quad (8)$$

Where $\overline{g_r}$ represents the estimated pixel values obtained through MAP optimization

After optimization, the values of *gr*(*x*,*y*) that minimize the objective function are extracted as the final pixel values:

$$g_{extracted}(x,y) = \overline{g_r}(x,y) \quad (9)$$

$g_{extracted}(x,y)$ Represents the extracted pixel values.

Mathematically, for each pixel (*x*,*y*), the noisy pixel value *N*(*x*,*y*) is given by:

$$N(x,y) = g_{extracted}(x,y) + \eta(x,y) \quad (10)$$

Where N(x,y) is the noisy pixel value at location (x,y) and $g_{extracted}(x,y)$ is the pixel value extracted from the previous step.

η(x,y) represents random values

To further smooth the noisy image and reduce noise, we apply Additional Gaussian filtering in the Process flow to the image with noise. The Gaussian filtering operation can be represented as

$$S_{ma}(x,y) = N(x,y)\ G_F(x,y) \quad (11)$$

Where S_{ma} *represents Smooth image with additional Filtering*

Apply blind deconvolution to the filtered image. The blind deconvolution problem can be mathematically formulated as follows:

$$g_{rs}(x,y) = (f(x,y)\ \circledast k(x,y)) + \eta(x,y) \quad (12)$$

Where *gr*(*x*,*y*) is the restored image obtained from the previous step (with noise reduced and additional smoothing), *f*(*x*,*y*) is the estimated original image, *k*(*x*,*y*) is the estimated blur kernel, *η*(*x*,*y*) represents the remaining noise.

Perform unsharp masking on the deconvolved image. Let *I*(*x*,*y*) be the deconvolved image obtained in the previous step. The unsharp masking operation can be mathematically represented as follows:

$$U(x,y) = I(x,y) - \lambda \cdot S(x,y) \quad (13)$$

Where U(x,y) is the unsharp masked image, I(x,y) is the deconvolved image, S(x,y) is a smoothed version of the deconvolved image (blurred image), λ is a scaling factor that controls the strength of enhancement. Calculate the noise ratio of the image:

$$noise\ ratio = \frac{standard\ deviation(image)}{mean(image)} \quad (14)$$

To eliminate the pixel noise ratio, we can use the following mathematical representation

$$U(x,y) = sign\big(D(x,y)\big) \circledast \max\big(abs\big(U(x,y)\big) - threshold, 0\big) \quad (15)$$

where threshold is a threshold value calculated as:

$$threshold = 3 \times noise\_ratio \times max(abs(U(x,y))) \quad (16)$$

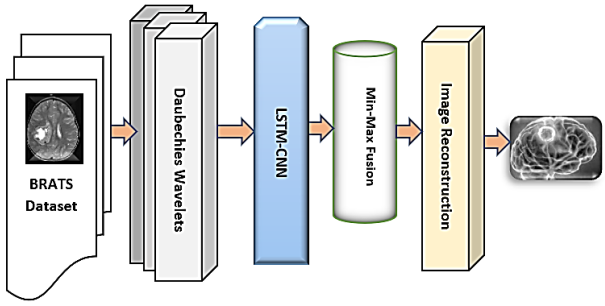

Figure. 2 EI-Fusion-Net model

Create a complementary image from the processed image. Apply Daubechies wavelet transform for image fusion. Utilize Min-Max fusion in combination with a LSTM-CNN architecture. Thus, the Name of the Model is Enhanced Image Fusion using Daubechies Wavelet and LSTM-CNN (EI-Fusion-Net) as shown in Fig. 2 as it conveys the concept of a novel image fusion approach that makes use of specific wavelet transform techniques and a fusion network architecture capable of capturing both spatial and temporal information for improved results.

The simple algorithm of the proposed model provided below in a stepwise manner.

Algorithm: EI-Fusion-Net

```
% Step a: Daubechies Wavelet Transform
input_image = imread('your_image_path.jpg'); % Load your input image
wavelet_level = 3; % Choose the level of wavelet decomposition
% Apply Daubechies wavelet transform
[coeffs, ~] = wavedec2(input_image, wavelet_level, 'db1');

% Step b: LSTM-CNN Model
% Define LSTM-CNN architecture using MATLAB Neural Network Toolbox

% Step c: Enhanced Image Fusion Net (EI-Fusion-Net)
% Assuming you have the LSTM-CNN model and coefficients from wavelet transform
% Concatenate or combine the results in a meaningful way

% Step d: Min-Max Fusion Technique
% Assuming you have processed image (from EI-Fusion-Net) and complementary image
fused_image = min(input_image, complementary_image) + max(input_image, complementary_image);
% Display the final fused image
imshow(fused_image);
```

This fusion technique combines the processed image and its complementary image to reconstruct the final image. Display the reconstructed version of the image resulting from the fusion process. This reconstructed image represents a combination of enhanced features and complementary information using the specified fusion technique. Obtain the Reconstructed Image and Carry out the Performance evaluation for parameters. Their respective formulae are provided below

Computational Time (msec):

$$T = End\ Time - Start\ Time \tag{17}$$

Computational Overhead (kb):

$$O = Memory\ Usage\ After\ Reconstruction - Memory\ Usage\ Before \tag{18}$$

$$PSNR = 10\ log10\left(\frac{(L^2)}{MSE}\right) \tag{19}$$

Where L is the maximum pixel value

The mean squared error, abbreviated as MSE, compares the original image to the one that was reconstructed.

$$MSE = \left(\frac{1}{(m*n)}\right) \Sigma\left[\Sigma\left(I(x,y) - R(x,y)\right)^2\right] \tag{20}$$

I(x, y) - Original Image Pixel values whereas R(x, y) denotes pixel values for a corresponding reconstructed Image.

$$SSIM = \frac{(2\,\mu_x\,\mu_y + C1)\,(2\,\sigma_{xy} + C2)}{(\mu_x^2 + \mu_y^2 + C1)\,(\sigma_x^2 + \sigma_y^2 + C2)} \tag{21}$$

Where μ is the mean value and $\sigma\ is\ the\ standard\ Deviation,$ C1 and C2 are constants

4. Result and analysis

The original brain MRI scan image obtained from the BRATS dataset [27] is shown in Fig. 3, it may also contain noise and artefacts that must be addressed in subsequent processing steps.

Fig. 4 shows the resized image obtained after resizing the original image to the desired dimensions. Fig. 5 shows the grayscale version of the resized image.

Table 1. Performance Parameters for Samples of Brain Tumor Images

	BRATS Brain Scan images MRI Scans				
Parameters	**BRATS Sample 1**	**BRATS Sample 2**	**BRATS Sample 3**	**BRATS Sample 4**	**BRATS Sample 5**
Computational Time (msec)	2.6122	2.564	2.562	2.631	2.5921
Computational Overhead (kb)	25.543	25.733	25.6913	25.512	25.2456
PSNR (db)	48.42	48.12	48.18	48.04	48.23
MSE	10.14	10.62	10.55	11.09	12.11
SSIM	0.992	0.988	0.983	0.987	0.981

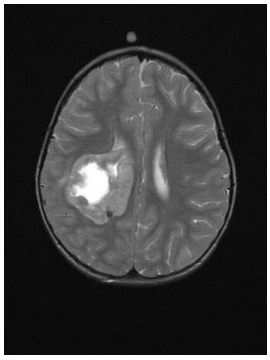

Figure. 3 Original Image

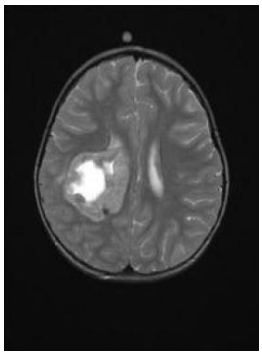

Figure. 4 Resized Image

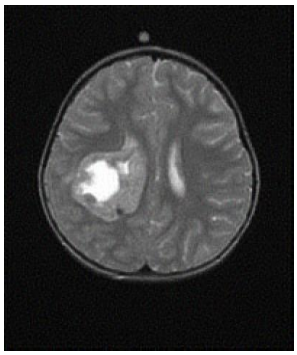

Figure. 9 Unsharp masking

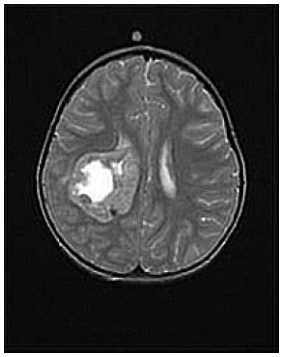

Figure. 10 Pixel noise ratio elimination

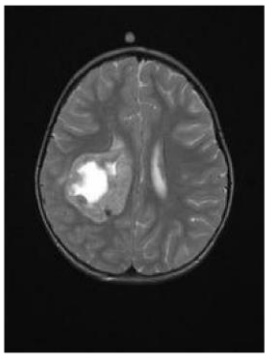

Figure. 5 Grayscale

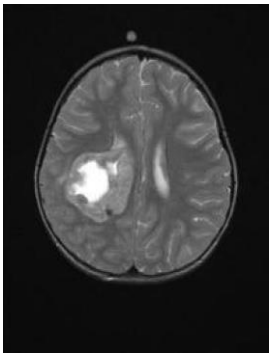

Figure. 6. Filtered image

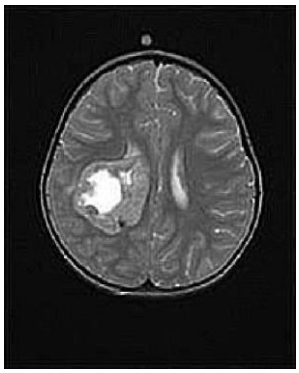

Figure. 11 Reconstructed image

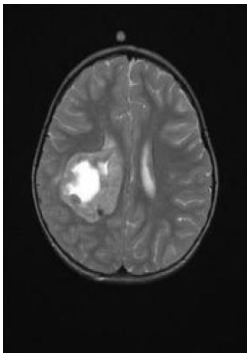

Fig. 7 Resultant of Deconvolution

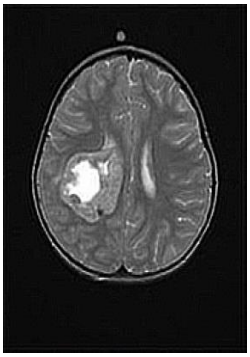

Figure. 8 Resultant of Pixel Extraction

Fig. 6 shows the outcome of applying a Gaussian filter to a grayscale image. This filtering step aims to reduce noise and create a smoother image representation. Fig. 7 shows the result of Wiener deconvolution applied to the filtered image.

Fig. 8 is the image after Maximum A Posteriori (MAP) pixel extraction.

The result of the unsharp masking step applied to the deconvolved image is shown in Fig. 9. In Fig. 10, we see the result of removing the pixel noise ratio.

Fig. 11 depicts the reconstructed image subsequent to the implementation of enhancements on the initial brain MRI scan. The methodology-processed brain tumor image samples' critical performance parameters are detailed in Table 1. The aforementioned metrics comprise computational time, computational overhead, MSR, PSNR and SSIM. PSNR values in the vicinity of 48 dB are suggestive of higher image quality. Sample 1, with a PSNR of 48.42 dB, demonstrates exceptional quality in reconstruction. Additionally, computational overhead (kb) is evaluated as a significant metric in Table 1 [11].

Finally, the SSIM (Structural Similarity Index) measures image quality by comparing the reconstructed and original images and has a value of 0.992. Figs. 12 and 13 show key performance parameters and plots for evaluating the brain tumour image processing methodology and model. Fig. 12 shows PSNR, MSE, and Computational Overhead for various samples. Sample 1's

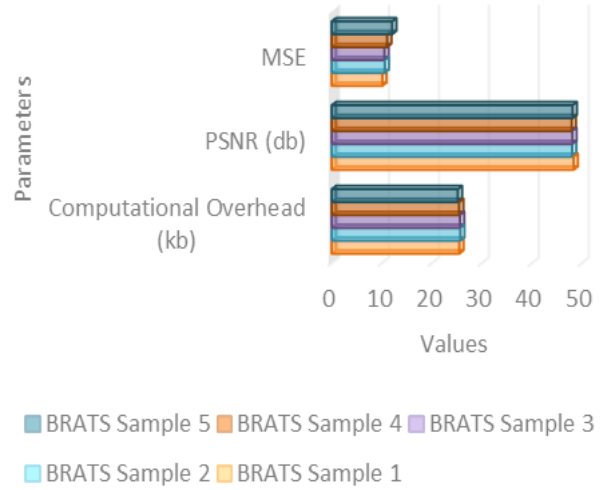

Figure. 12 Performance parameters PSNR, MSE and Computational Overhead

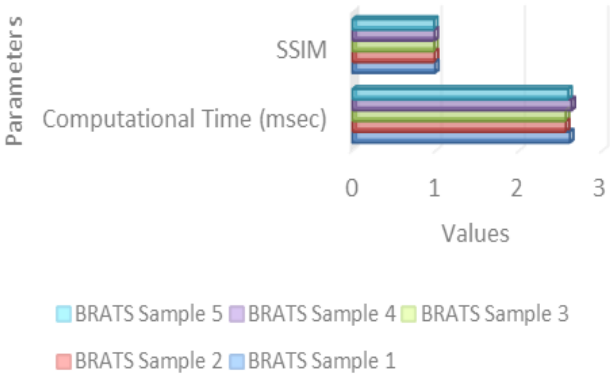

Figure. 13 Performance parameters Computational Time and SSIM

Table 2. PSNR and SSIM comparative assessment

Methods	PSNR (db)	SSIM
SepGAN [19]	44.22	0.985
DRFDCAN [20]	34.20	0.9468
GATE-Net [21]	36.81	0.978
Feature Fusion [22]	29.46	0.89
Novel GAN [23]	38.83	0.95
FDA-CNN [24]	41.75	0.98
Hybrid compressive sensing [25]	41.68	0.975
MRBT-SR-GAN [26]	29.42	0.986
Proposed Method (EI-Fusion-Net)	**48.42**	**0.992**

PSNR of 63.25 dB indicates superior image quality compared to other samples. Sample 1 has an impressively low MSE of 10.14, indicating the quality of the reconstructed image. Sample 4 has the lowest Computational Overhead (25.512 kb), indicating efficient memory and computational resource management.

Computational Time (milliseconds) and SSIM values for various samples are shown in Fig. 13. The most efficient image reconstruction method is Sample 3, which takes 2.562 msec. Sample 1, however, performs best with an SSIM value of 0.992, indicating high structural similarity between the reconstructed and original images.

Sample 1 has the highest PSNR, SSIM, and MSE, indicating superior image quality. Sample 3 has the fastest computation. Sample 4 has the lowest computational overhead, indicating memory efficiency.

Table 2 presents a comprehensive comparison of various image enhancement and reconstruction methods based on PSNR and SSIM metrics. These metrics serve as fundamental benchmarks for assessing the quality of reconstructed images, with higher values indicating greater fidelity to the original signal and structural similarities. Among the methods tested, the proposed EI-Fusion-Net achieved the highest PSNR of 48.42 dB and SSIM of 0.992, demonstrating its exceptional ability to generate high-quality images while preserving fine structural details. In contrast, methods such as Feature Fusion and MRBT-SR-GAN have lower PSNR and SSIM values, indicating poorer performance in terms of both signal fidelity and structural similarity, emphasizing the importance of advanced techniques such as EI-Fusion-Net for superior image reconstruction tasks.

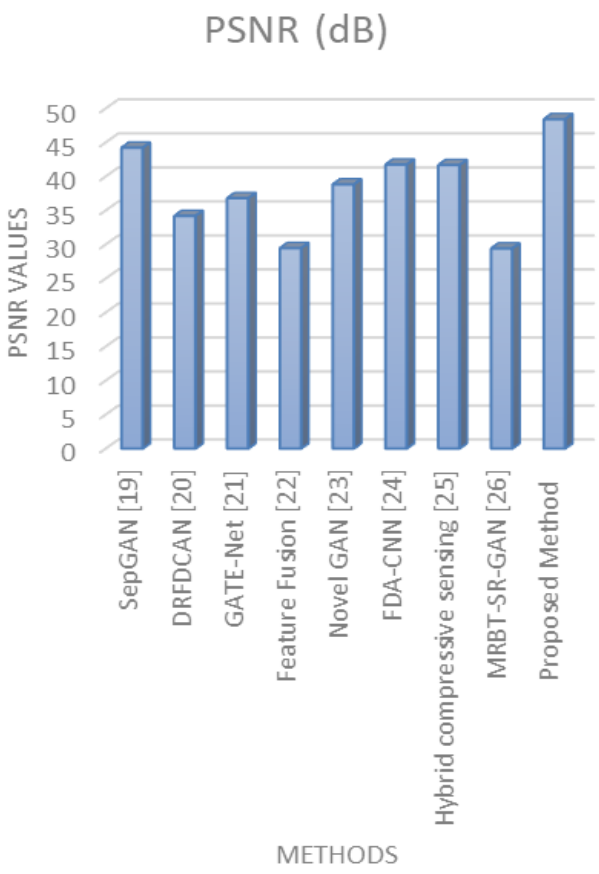

Figure. 14 Plot of comparative analysis of PSNR

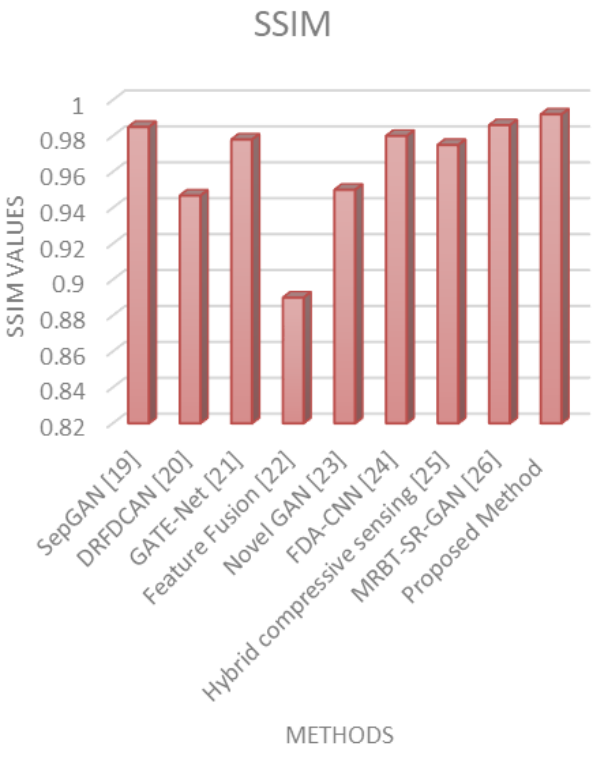

Figure. 15 Plot of comparative analysis of SSIM

Table 2's findings highlight the importance of Similarly, in Fig. 15, which depicts the Comparative Analysis of SSIM (Structural Similarity Index advancement of image processing and novel approaches such as EI-Fusion-Net in the reconstruction. By outperforming existing methods in terms of PSNR and SSIM scores, EI-Fusion-Net demonstrates its superiority and fidelity in medical imaging. These findings are useful for researchers and practitioners working to develop more effective and reliable image reconstruction techniques, ultimately contributing to advances in fields that rely on high-quality image data for analysis and decision-making.

Fig. 14 depicts the Comparative Analysis of PSNR (Peak Signal-to-Noise Ratio), with the X-axis denoting the various methods considered and the Y-axis representing the corresponding PSNR values. Given the values in Table 2, it is clear that the proposed method (EI-Fusion-Net) achieves the highest PSNR of all methods listed, as evidenced by the tallest bar. This suggests that the EI-Fusion-Net outdoes others in terms of signal quality and noise reduction, making it a promising candidate for image enhancement and reconstruction tasks.

Measure), the X-axis represents the methods used, and the Y-axis displays the SSIM values. Once again, the proposed method has the highest SSIM value, indicating that it preserves structural details better than other methods. This reinforces the proposed EI-Fusion-Net's ability to maintain structural similarity with the original image, resulting in higher-quality reconstructed images.

5. Conclusion and summary

To summarize, this study represents a significant advancement in the field of medical image processing, specifically the detection of brain tumors using MRI scans. The study introduces a novel approach to improving tumor detection accuracy and efficacy by leveraging cutting-edge techniques and methodologies. Using the BRATS dataset, the proposed method incorporates a number of sophisticated techniques, including Maximum A Posteriori (MAP) optimization, Wiener deconvolution, and the EI-Fusion-Net deep learning model. Additionally, preprocessing steps such as resizing, grayscale conversion, and Gaussian filtering are used to improve the quality of the MRI images. The obtained results show exceptional performance, with a PSNR of 48.42 dB and a SSIM of 0.992, which outperforms existing methods on BRATS dataset. This demonstrates the effectiveness of the EI-Fusion-Net model in seamlessly integrating disparate data

and represents significant progress in brain tumor detection using advanced medical image processing techniques. Overall, this study paves the way for future advances in medical imaging technology, which will lead to better diagnostic accuracy and patient care in the field of neuroscience.

Notations List :

- g(x, y) is the resized image
- f(x, y) is the original image
- gray (x, y) is the resulting grayscale image
- $S_m(x, y)$ is the resulting smoothed image
- $G_F(x, y)$ is the Gaussian kernel
- (x, y) are the coordinates in the kernel
- σ (sigma) controls the spread or standard deviation of the Gaussian distribution
- π (pi) is the mathematical constant
- e is the base of the natural logarithm.
- G(u,v) is the estimated Fourier transform of the original image.
- $\overline{H}(u, v)$ is the complex conjugate of the PSF's frequency response.
- K is a constant (Wiener regularization parameter),
- $|H(u, v)|^2$ represents the magnitude of the PSF's frequency response squared.
- N(u,v) represents the noise power spectral density
- g_r (x,y) is the restored image in spatial domain
- $E(gr)$ is the energy or cost associated with the restored image $gr(x,y)$
- $P(gr \mid \text{observed data})$ represents the likelihood term, which measures how well the restored image fits the observed data
- $P(gr \mid \text{prior})$ represents the prior term, which encodes prior knowledge or constraints on the image.
- $g_{extracted}(x, y)$ Represents the extracted pixel values.
- N(x,y) is the noisy pixel value at location (x,y)
- η(x,y) represents random values
- $S_{ma}(x, y)$ represents Smooth image with additional Filtering
- U(x,y) is the unsharp masked image
- I(x,y) is the deconvolved image
- S(x,y) is a smoothed version of the deconvolved image (blurred image)
- λ is a scaling factor that controls the strength of enhancement.

Conflicts of Interest

The authors affirm that they are aware of no personal or financial conflicts of interest that might have affected the research described in this paper

Author Contributions

BSH. Shayeez Ahamed -Conceptualization, Data curation Formal analysis, Radhika Baskar-Methodology, Software Writing, original draft, investigation, resources. G. Nalinipriya-Writing—review and editing, visualization, supervision, project administration.

References

[1] Q.T. Ostrom, H. Gittleman, P. Liao, T. V. Koval, Y. Wolinsky, C. Kruchko, and J. S. B. Sloan, "Cbtrus statistical report: primary brain and other central nervous system tumors diagnosed in the United States in 2010-2014", *Neuro-Oncology*, Vol. 19, Suppl_5, pp. v1-v88, 2017.

[2] E. B. Claus, K. M. Walsh, J. K. Wiencke, A. M. Molinaro, J. L. Wiemels, J. M. Schildkraut, M. L. Bondy, M. Berger, R. Jenkins, and M. Wrensch, "Survival and low-grade glioma: the emergence of genetic information", *Neurosurgical Focus*, Vol. 38, No. 1, p. E6, 2015.

[3] S. Chen, C. Ding, and M. Liu, "Dual-force convolutional neural networks for accurate brain tumor segmentation", *Pattern Recognition*, Vol. 88, pp. 90-100, 2019.

[4] L. S. Chow, H. Rajagopal, and R. Paramesran, "Correlation between subjective and objective assessment of magnetic resonance (MR) images", *Magnetic Resonance Imaging*, Vol. 34, pp. 820-831, 2016.

[5] L. Bao, W. Liu, Y. Zhu, Z. Pu, and I. E. Magnin, "Sparse representation based MRI denoising with total variation", In: *Proc. of the 2008 9th International Conf on Signal Processing*, Beijing, China, pp. 2154-2157, 2008.

[6] K. L. Chaichana, S. L. Parker, A. Olivi, and A. Q. Hinojosa, "Long-term seizure outcomes in adult patients undergoing primary resection of malignant brain astrocytomas", *Journal of Neurosurgery*, Vol. 111, No. 2, pp. 282-292, 2009.

[7] X. Yang and B. Fei, "A wavelet multiscale denoising algorithm for magnetic resonance (MR) images", *Measurement Science and Technology*, Vol. 22, No. 2, p. 025803, 2011.

[8] J. Andrew, T. S. R. Mhatesh, R. D. Sebastin, K. M. Sagayam, J. Eunice, M. Pomplun, and H.

Dang, "Super-resolution reconstruction of brain magnetic resonance images via lightweight autoencoder", *Informatics in Medicine Unlocked*, Vol. 26, p. 100713, 2021.

[9] M. B. Pinkham, G. A. Whitfield, and M. Brada, "New developments in intracranial stereotactic radiotherapy for metastases", *Clinical Oncology*, Vol. 27, No. 5, pp. 316-323, 2015.

[10] A. Aghabiglou and E. M. Eksioglu, "Projection-based cascaded u-net model for MR image reconstruction", *Computer Methods and Programs in Biomedicine*, Vol. 207, p. 106151, 2021.

[11] X. Liu, J. Wang, S. Lin, S. Crozier, and F. Liu, "Optimizing multicontrast MRI reconstruction with shareable feature aggregation and selection", *NMR in Biomedicine*, Vol. 34, p. e4540, 2021.

[12] R. Souza and R. Frayne, "A hybrid frequency-domain/image-domain deep network for magnetic resonance image reconstruction", In: *Proc of the 2019 32nd SIBGRAPI Conf on Graphics, Patterns and Images*, Rio de Janeiro, Brazil, pp. 257-264, 2019.

[13] T. Zhou, S. Ruan, and S. Canu, "A review: deep learning for medical image segmentation using multi-modality fusion", *Array*, Vol. 6, p. 100004, 2019.

[14] G. Litjens, T. Kooi, B. E. Bejnordi, A. A. A. Setio, F. Ciompi, M. Ghafoorian, J. A. W. M. V. D. Laak, B. V. Ginneken, and C. I. Sánchez, "A survey on deep learning in medical image analysis", *Medical Image Analysis*, Vol. 42, pp. 60-88, 2017.

[15] J. M. Miller, C. E. Rochitte, M. Dewey, et al., "Diagnostic performance of coronary angiography by 64-row CT", *New England Journal of Medicine*, Vol. 359, pp. 2324-2336, 2008.

[16] J. Z. Cheng, D. Ni, Y.H. Chou, et al., "Computer-Aided Diagnosis with Deep Learning Architecture: Applications to Breast Lesions in US Images and Pulmonary Nodules in MRI Scans", *Scientific Reports*, Vol. 6, p. 24454, 2016.

[17] H. B. Yedder, B. Cardoen, and G. Hamarneh, "Deep learning for biomedical image reconstruction: a survey", *Artificial Intelligence Review*, Vol. 54, No. 1, pp. 215-251, 2021.

[18] D. Ardila, A. P. Kiraly, S. Bharadwaj, et al., "End-to-end lung cancer screening with three-dimensional deep learning on low-dose chest computed tomography", *Nature Medicine*, Vol. 25, No. 6, pp. 954-961, 2019.

[19] J. Xu, W. Bi, L. Yan, H. Du, and B. Qiu, "An Efficient Lightweight Generative Adversarial Network for Compressed Sensing Magnetic Resonance Imaging Reconstruction", *IEEE Access*, Vol. 11, pp. 24604-24614, 2023.

[20] S. Umirzakova, S. Mardieva, S. Muksimova, S. Ahmad, and T. Whangbo, "Enhancing the Super-Resolution of Medical Images: Introducing the Deep Residual Feature Distillation Channel Attention Network for Optimized Performance and Efficiency", *Bioengineering*, Vol. 10, No. 11, p. 1332, 2023.

[21] Y. Li, J. Yang, T. Yu, J. Chi, and F. Liu, "Global attention-enabled texture enhancement network for MR image reconstruction", *Magnetic Resonance in Medicine*, Vol. 90, No. 5, pp. 1919-1931, 2023.

[22] T. Zhou, "Feature fusion and latent feature learning guided brain tumor segmentation and missing modality recovery network", *Pattern Recognition*, Vol. 141, p. 109665, 2023.

[23] W. Ahmad, H. Ali, Z. Shah, et al., "A new generative adversarial network for medical images super resolution", *Scientific Reports*, Vol. 12, p. 9533, 2022.

[24] M. Hossain, K. Kwon, S. M. Imtiaz, O. S. Nam, S. H. Jeon, and N. Kim, "De-Aliasing and Accelerated Sparse Magnetic Resonance Image Reconstruction Using Fully Dense CNN with Attention Gates", *Bioengineering*, Vol. 10, p. 22, 2022.

[25] N. Shilpa and C. Veena, "A Hybrid Compressive Sensing Network for ROI-based Medical Image Recovery", *Electrical and Electronics Engineering An International Journal*, Vol. 10, No. 3, p. 102, 2023.

[26] Z. Zhou, A. Ma, Q. Feng, et al., "Super-resolution of brain tumor MRI images based on deep learning", *Journal of Applied Clinical Medical Physics*, Vol. 23, No. 11, p. e13758, 2022.

[27] B. Menze, A. Jakab, S. Bauer, J. K. Cramer, K. Farahani, J. Kirby, Y. Burren, N. Porz, J. Slotboom, R. Wiest, L. Lanczi, L. Gerstner, M. A. Weber, T. Arbel, B. Avants, N. Ayache, P. Buendia, L. Collins, N. Cordier, and K. Van Leemput, "The Multimodal Brain Tumor Image Segmentation Benchmark (BRATS)", *IEEE Transactions on Medical Imaging*, Vol. 99, 2014.